Electronic Supplementary Material (ESI) for Dalton Transactions.

Supporting Information for

Modulating crystal and electronic structure of NiFe-MOFs by inorganic acid for highly efficient electrochemical water oxidation

Fang Wu,[a,b] Qiulin Li,[c] Hu Guo,[a] Suwei Wang,[a] Gazi Hao,[a] Yubing Hu,[a] Guangpu Zhang, [a] Wei Jiang*[a]

E-mail: superfine_jw@126.com

[a]School of Chemical Engineering, Nanjing University of Science and Technology, Nanjing 210094, China. E-mail: superfine_jw@126.com.

[b]School of Material and Chemical Engineering, Bengbu University, Bengbu, Anhui 233000, China.

[c]Jiangsu Key Laboratory for Environment Functional Materials, Suzhou University of Science and Technology, Suzhou 215009, China.

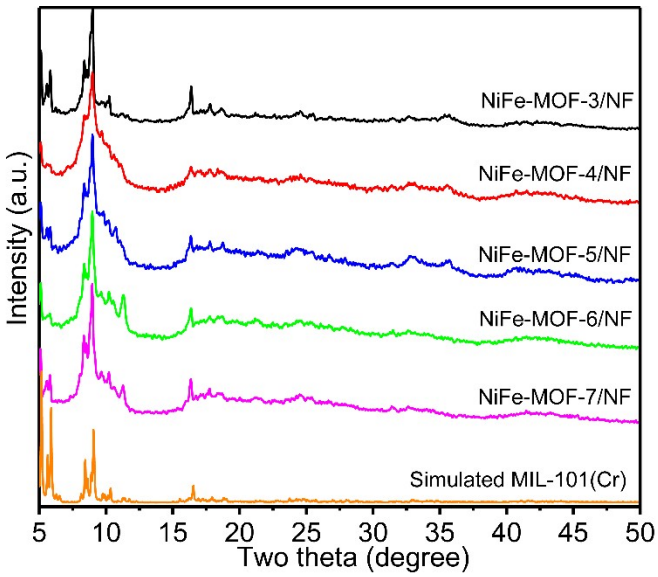

Fig. S1 PXRD patterns of NiFe-MOF-n/NF (x = 3, 4, 5, 6, 7) and simulated MIL-101(Cr).

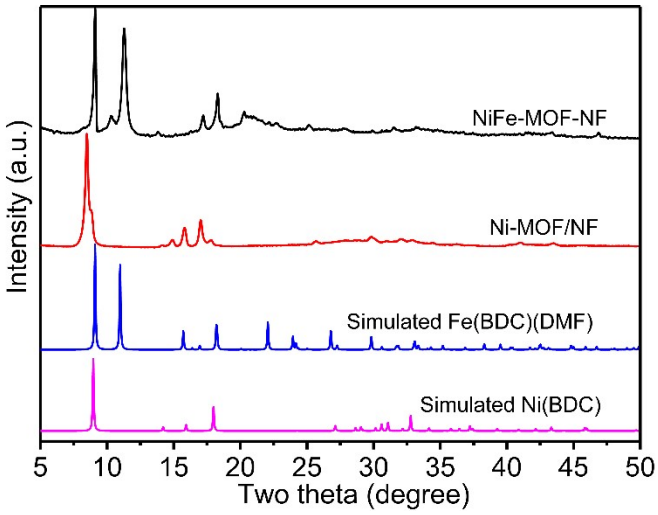

Fig. S2 PXRD patterns of Ni-MOF/NF, NiFe-MOF-NF, simulated Ni(BDC) and simulated Fe(BDC)(DMF).

Note: The XRD pattern of Ni-MOF/NF should be assigned to Ni(BDC).[1] Notably, the diffraction peaks of Ni-MOF/NF were shifted to lower angles compared to the simulated pattern for Ni(BDC) possibly due to the influence of solvent.[2] As shown in **Fig. S2**, the diffraction peaks of obtained NiFe-MOF/NF matched well with Fe(BDC)(DMF) when iron and nickel salt were added during hydrothermal process.

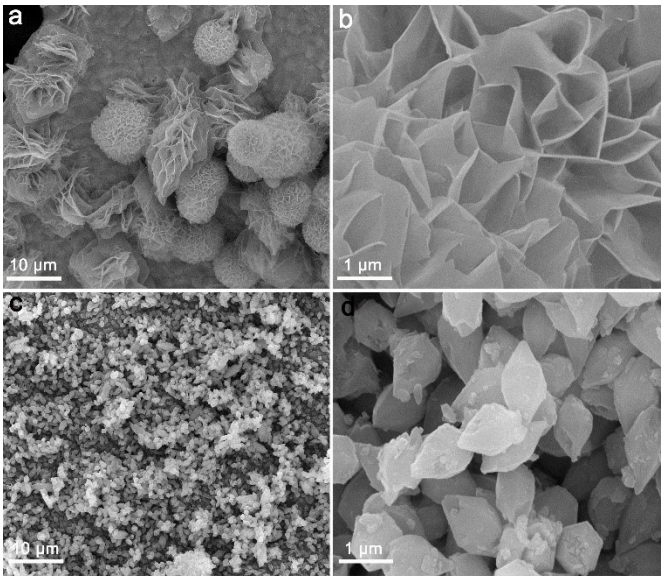

Fig. S3 SEM images of (a, b) Ni-MOF/NF and (c, d) NiFe-MOF-NF.

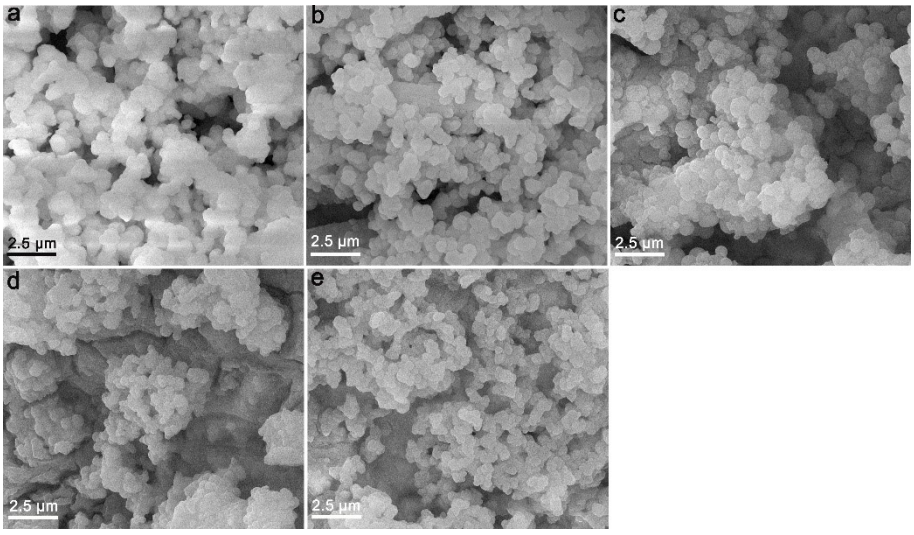

Fig. S4 SEM images of (a) NiFe-MOF-3/NF, (b) NiFe-MOF-4/NF, (c) NiFe-MOF-5/NF, (d) NiFe-MOF-6/NF and (e) NiFe-MOF-7/NF.

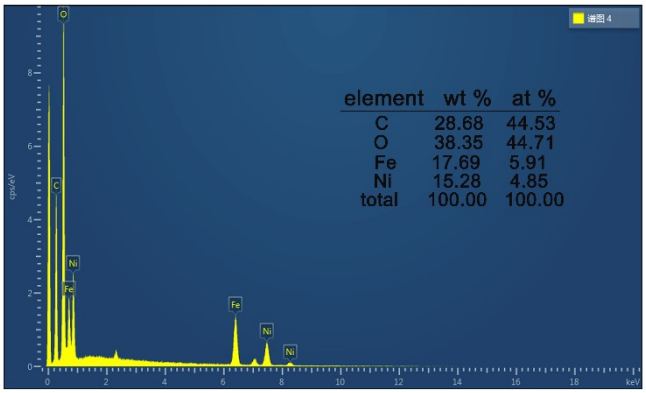

Fig. S5 SEM-EDX spectra of NiFe-MOF-2/NF.

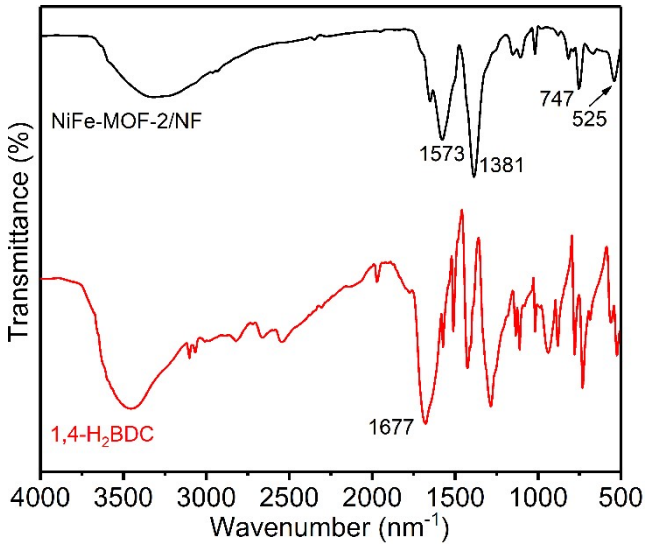

Fig. S6 FT-IR spectrums of NiFe-MOF-2/NF and 1,4-H_2BDC.

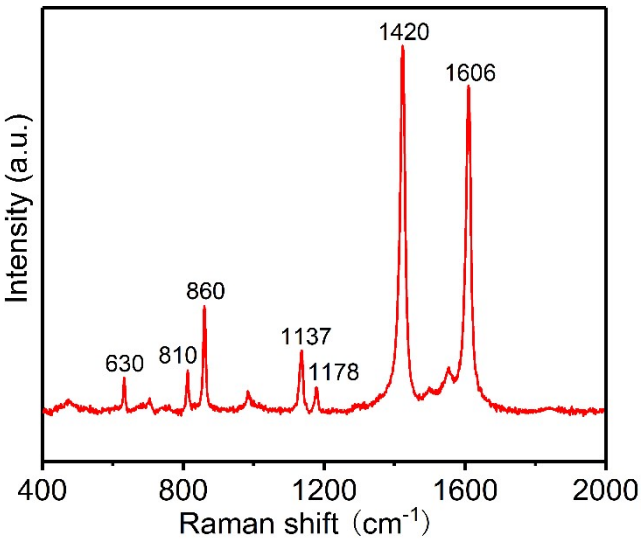

Fig. S7 Raman spectra of NiFe-MOF-2/NF.

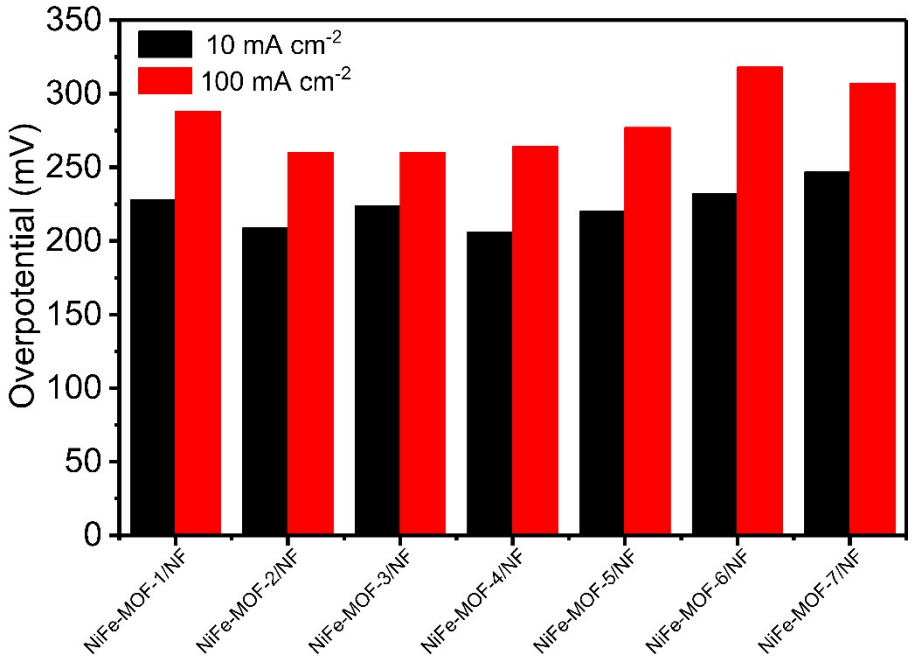

Fig. S8 The comparison of the overpotentials to reach the current densities of 10 and 100 mA cm^{-2}.

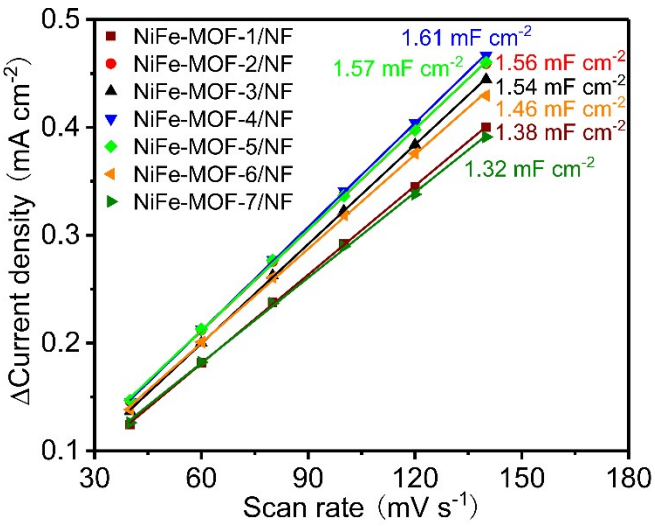

Fig. S9 The plots of ΔJ versus scan rates for NiFe-MOF-n/NF (n= 1-7).

Note: The ECSA of NiFe-MOF-n/NF (n = 1-7) were determined by CV at varying rates from 40 to 140 mV s^{-1}. The ECSA test of the NiFe-MOF-n/NF (n= 2, 3, 4, 5) show similar values, as shown in **Fig. S9**, indicating that the accessible catalytically surface area, and thus active sites in the four samples are close to each other.

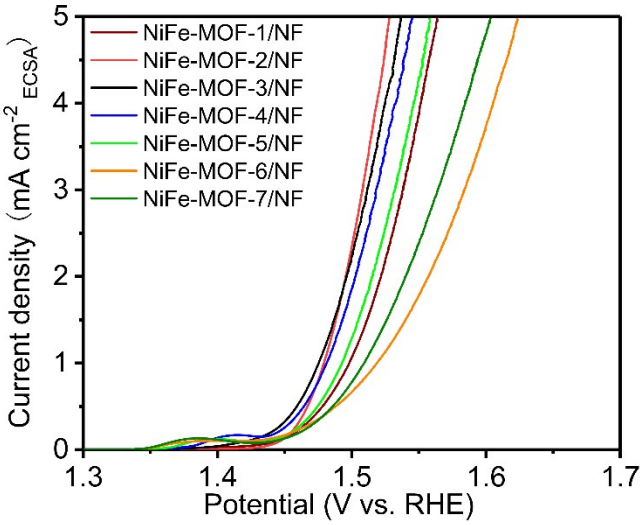

Fig. S10 ECSA-normalized polarization curves for NiFe-MOF-n/NF (n= 1-7).

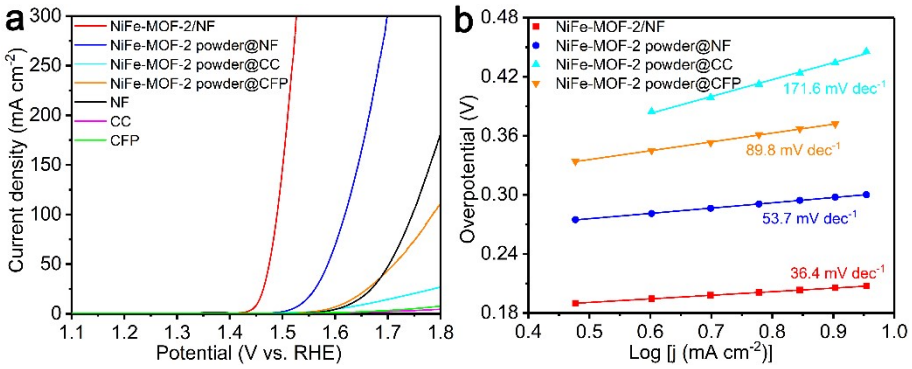

Fig. S11 (a) The LSV curves of NiFe-MOF-2/NF, NiFe-MOF-2 powder@NF, NiFe-MOF-2 powder@CC, NiFe-MOF-2 powder@CFP, NF, CC and CFP, (b) the corresponding Tafel slopes.

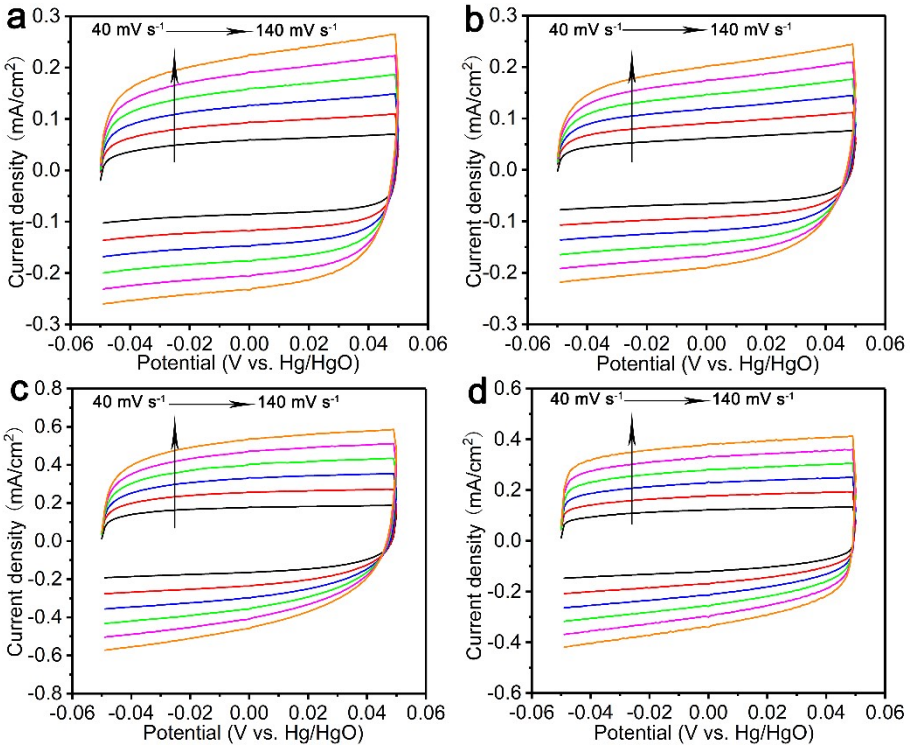

Fig. S12 CV curves of (a) NiFe-MOF-2/NF, (b) NiFe-MOF-2 powder@NF, (c) NiFe-MOF-2 powder@CC and (d) NiFe-MOF-2 powder@CFP at different scan rates in the potential range of -0.05–0.05 V vs Hg/HgO.

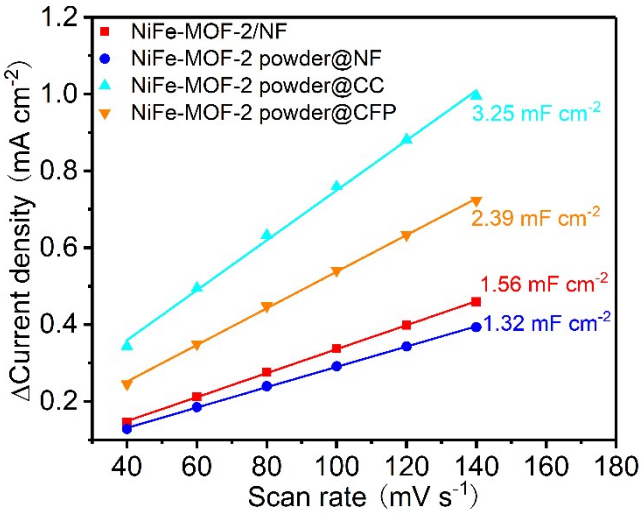

Fig. S13 Charging current density differences plotted against scan rates of NiFe-MOF-2/NF, NiFe-MOF-2 powder@NF, NiFe-MOF-2 powder@CC and NiFe-MOF-2 powder@CFP at 0.92 V vs. RHE.

Note: To explore the significant OER activity difference between NiFe-MOF-2/NF, NiFe-MOF-2 powder@NF, NiFe-MOF-2 powder@CC and NiFe-MOF-2 powder@CFP, ECSA were evaluated by C_{dl} through CV measurement (**Fig. S12** and **S13**). Although both NiFe-MOF-2 powder@CC and NiFe-MOF-2 powder@CFP have larger C_{dl} value (3.25 mF cm^{-2} and 2.39 mF cm^{-2}) compared with NiFe-MOF-2 powder@NF and NiFe-MOF-2/NF, the C_{dl} of NiFe-MOF-2 powder@CC and NiFe-MOF-2 powder@CFP mostly derived from carbon supports.3 NiFe-MOF-2/NF shows a higher C_{dl} (1.56 mF cm^{-2}) than that of NiFe-MOF-2 powder@NF (1.32 mF cm^{-2}), indicating more accessible active sites of NiFe-MOF-2/NF.

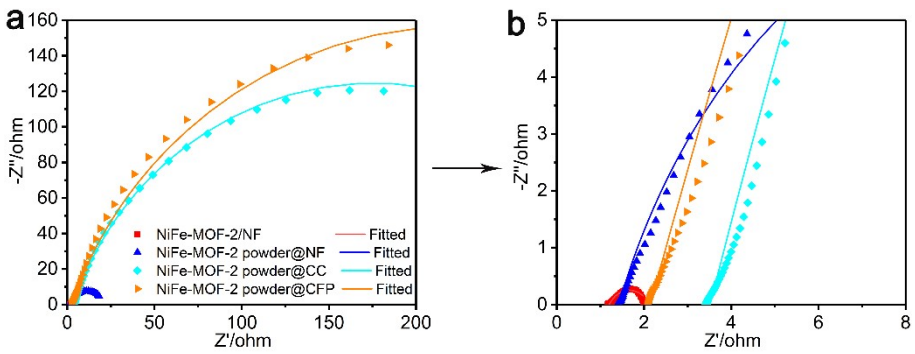

Fig. S14 (a) Nyquist plots of electrodes at the overpotential of 250 mV, (b) enlarge Nyquist plots in the high frequency region.

Note: To further investigate the significant difference in OER performance among the four samples, EIS were carried out (**Fig. S14**). As expected, NiFe-MOF-2/NF exhibits the smallest semicircle radius in contrast to NiFe-MOF-2 powder@substrate samples, implying the lowest R_{ct} and fastest electron transfer kinetics. In addition, NiFe-MOF-2 powder@NF possesses much smaller R_{ct} than NiFe-MOF-2 powder@CC and NiFe-MOF-2 powder@CFP, which indicates that the improved OER performance of NiFe-MOF-2 powder@NF may result from enhanced conductivity of the NF substrate.

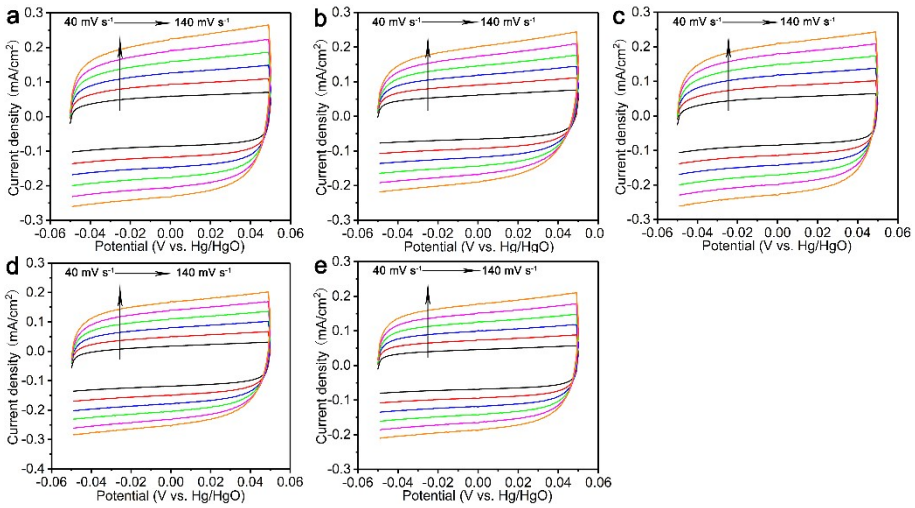

Fig. S15 CV curves of (a) NiFe-MOF-2/NF, (b) NiFe-MOF-2 powder@NF, (c) Fe-MOF/NF, (d) Ni-MOF/NF and (e) NiFe-MOF-NF at different scan rates in the potential range of -0.05–0.05 V vs Hg/HgO.

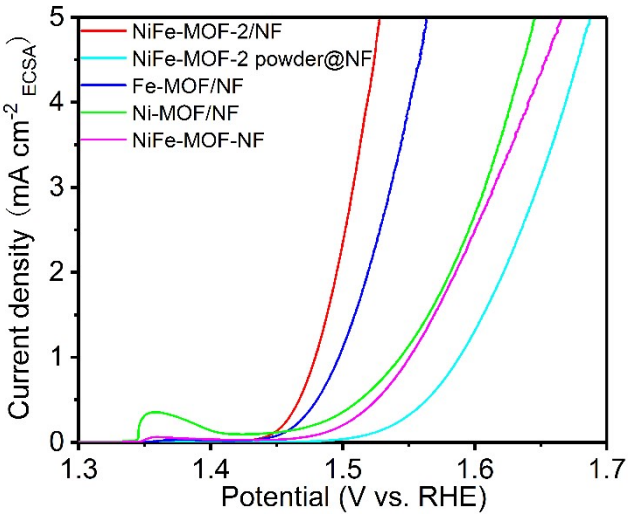

Fig. S16 ECSA-normalized polarization curves for NiFe-MOF-2/NF, NiFe-MOF-2 powder@NF, FeMOF/NF, Ni-MOF/NF and NiFe-MOF-NF.

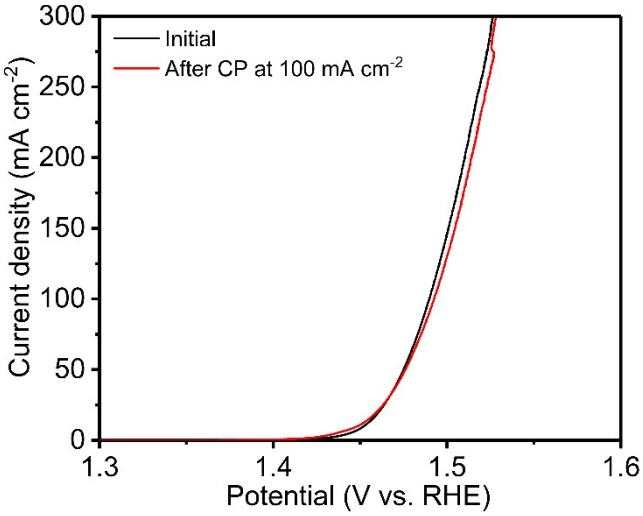

Fig. S17 LSV curves of NiFe-MOF-2/NF before and after stability test.

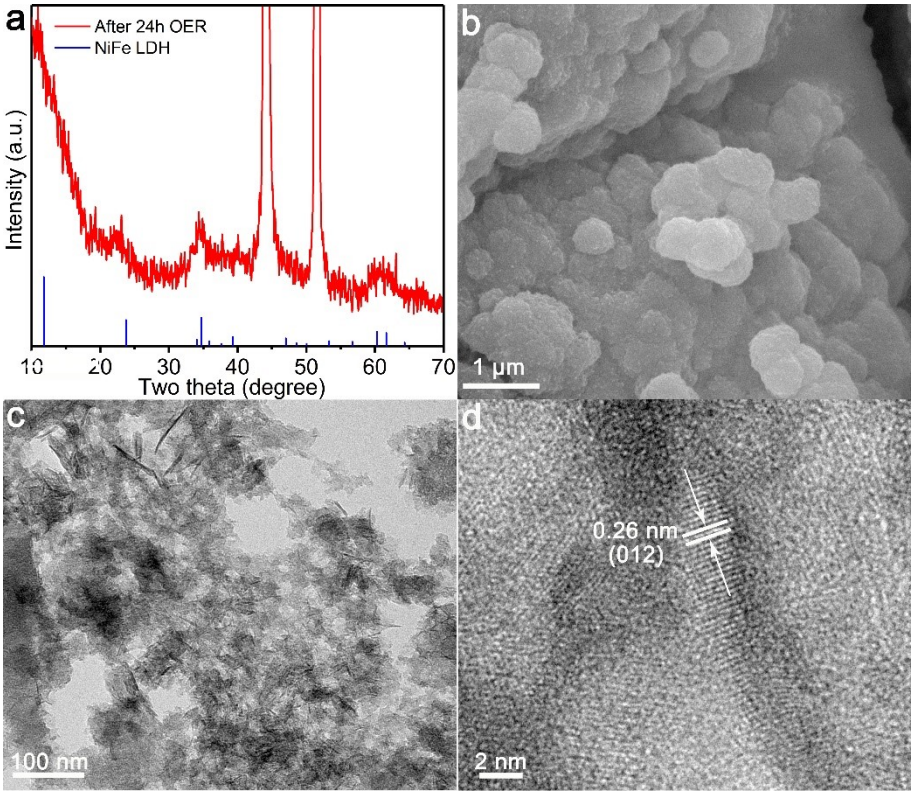

Fig. S18 (a) XRD patterns of NiFe-MOF-2/NF after stability test; (b) SEM, (c) TEM and (d) HRTEM images of NiFe-MOF-2/NF after stability test.

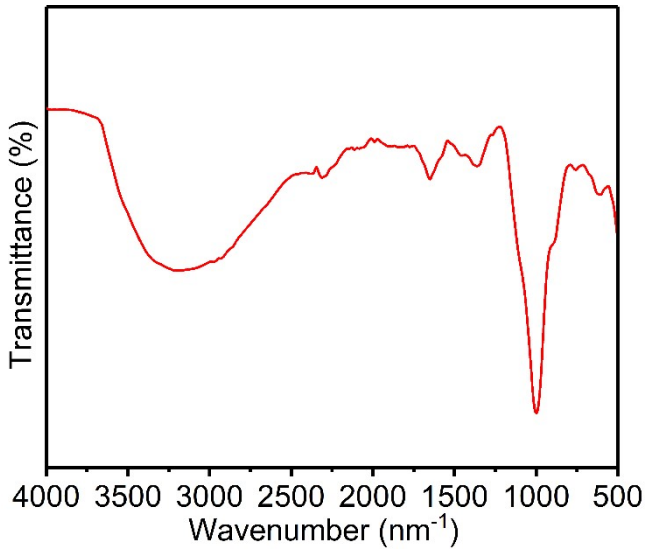

Fig. S19 FT-IR spectra of NiFe-MOF-2/NF after stability test.

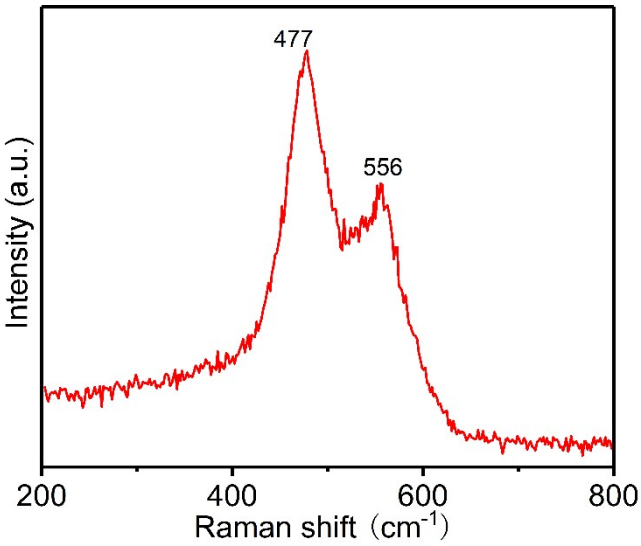

Fig. S20 Raman spectra of NiFe-MOF-2/NF after stability test.

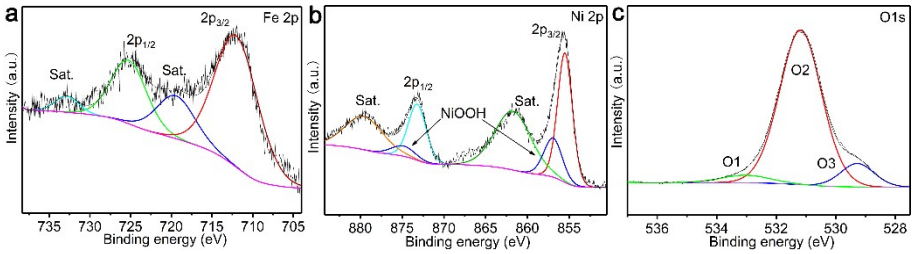

Fig. S21 High-resolution XPS spectra of (a) Fe 2p, (b) Ni 2p and (c) O 1s for NiFe-MOF-2/NF after stability test.

Table S1. Comparison of OER performance of NiFe-MOF-2/NF with various NiFe-based OER electrocatalysts in 1 M KOH.

Catalyst	Substrates	η@10 mA cm^{-2} mV	η@100 mA cm^{-2} mV	Tafel Slope mV dec^{-1}	Stability test	Reference
NiFe-MOF-2/NF	NF	209	260	36.4	24 h	This work
MIL-88A/$Ni(OH)_2$	CC	250	-	36.4	40 h	4
Ni_3S_2@$Fe(OH)_2$	GCE	230	288	33.1	300 h	5
Ni-Fe-MOFs NSs	GCE	221	-	56	20 h	6
$Fe_{7.2\%}$-Ni_3S_2 NSs/NF	NF	295	-	71	10 h	7
FeCo-MOF-EH/NF	NF	231	-	42	30 h	8
NiFe-NFF	NFF	227	253	38.9	15 h	9
Fe1Ni_2(BDC-NH_2)/NF	NF	228	-	30.3	12 h	10
(Fe-Ni)Co_x-OH/Ni_3S_2	NF	-	280	57	100 h	11
NiFeZr LDHs	NF	198	-	53.1	12 h	12
FeNi-HDNAs	NF	206	300	91.66	10 h	13
Ni_3Se_4@NiFe LDH/CFC	CFC	223	290	55.5	100 h	14
NiV-LDH@FeOOH	NF	-	297	57.3	20 h	15
Ni_2P@FePOxHy	NF	220	260	43	288 h	16
CoNiFe-OH-1M	NF	207	261	52.1	60 h	17
HO_{oct}-NFO NC/IF	IF	260	290	36.1	50 h	18

Supplementary references

1 B. Wang, J. Shang, C. Guo, J. Zhang, F. Zhu, A. Han and J. Liu, A General Method to Ultrathin Bimetal-MOF Nanosheets Arrays via In Situ Transformation of Layered Double Hydroxides Arrays, Small, 2019, **15**, 1804761.

2 J. Wang, Q. Zhong, Y. Xiong, D. Cheng, Y. Zeng, Y. Bu, Fabrication of 3D Co-doped Ni-based MOF hierarchical micro-flowers as a high-performance electrode material for supercapacitors, *Appl. Surf. Sci.*, 2019, **483**, 1158–1165.

3 J. Wang, F. Xu, H. Jin, Y. Chen and Y. Wang, Non-Noble Metal-based Carbon Composites in Hydrogen Evolution Reaction: Fundamentals to Applications, *Adv. Mater.*, 2017, **29**, 1605838.

4 Z. Qian, K. Wang, K. Shi, Z. Fu, Z. Mai, X. Wang, Z. Tang and Y. Tian, Interfacial electron transfer of heterostructured MIL-88A/$Ni(OH)_2$ enhances the oxygen evolution reaction in alkaline solutions, *J. Mater. Chem. A*, 2020, **8**, 3311–3321.

5 J. Li, F. Liu, M. Yu, H. Hu, H. Liu and F. Cheng, Interfacial Engineering of Ni−Fe Based Electrocatalysts for Robust Oxygen Evolution, *J. Phys. Chem. C*, 2021, **125**, 25383−25391.

6 F.-L. Li, P. Wang, X. Huang, D. J. Young, H.-F. Wang, P. Braunstein and J.-P. Lang, Large-Scale, Bottom-Up Synthesis of Binary Metal–Organic Framework Nanosheets for Efficient Water Oxidation, *Angew. Chem. Int. Ed.*, 2019, **58**, 7051–7056.

7 Y. Zhu, H. Yang, K. Lan, K. lqbal, Y. Liu, P. Ma, Z. Zhao, S. Luo, Y. Luo and J. Ma, Optimization of iron-doped Ni_3S_2 nanosheets by disorder engineering for oxygen evolution reaction, *Nanoscale*, 2019, **11**, 2355–2365.

8 J. Tian, F. Jiang, D. Yuan, L. Zhang, Q. Chen and M. Hong, Electric-Field Assisted In Situ Hydrolysis of Bulk Metal–Organic Frameworks (MOFs) into Ultrathin Metal Oxyhydroxide Nanosheets for Efficient Oxygen Evolution, *Angew. Chem. Int. Ed.*, 2020, **59**, 13101–13108.

9 C. Cao, D.-D. Ma, Q. Xu, X.-T. Wu and Q.-L. Zhu, Semisacrificial Template Growth of Self-Supporting MOF Nanocomposite Electrode for Efficient Electrocatalytic Water Oxidation, *Adv. Funct. Mater.*, 2019, **29**, 1807418.

10 J. Ma, X. Bai, W. He, S. Wang, L. Li, H. Chen, T. Wang, X. Zhang, Y. Li, L. Zhang, J. Chen, F. Meng and Y. Fu, Amorphous FeNi-bimetallic infinite coordination polymers as advanced electrocatalysts for the oxygen evolution reaction, *Chem. Commun.*, 2019, **55**, 12567–12570.

11 Q. Che, Q. Li, X. Chen, Y. Tan, X. Xu, Assembling amorphous (Fe-Ni)Co_x-OH/Ni_3S_2 nanohybrids with S-vacancy and interfacial effects as an ultra-highly efficient electrocatalyst: Inner investigation of mechanism for alkaline water-to-hydrogen/oxygen conversion, *Appl. Catal. B- Environ.*, 2020, **263**, 118338.

12 R. Li, Y. Wang, W. Li, S. Zhou, P. Tian, H. Gao, X. Liu and J. Zang, Ternary NiFeZr layered double hydroxides: a highly efficient catalyst for the oxygen evolution reaction, *Chem. Commun.*, 2019, **55**, 13370–13373.

13 N. Yu, W. Cao, M. Huttula, Y. Kayser, P. Hoenicke, B. Beckhoff, F. Lai, R. Dong, H. Sun, B. Geng, Fabrication of FeNi hydroxides double-shell nanotube arrays with enhanced performance for oxygen evolution reaction, *Appl. Catal. B-Environ.*, 2020, **261**, 118193.

14 T. Zhang, L. Hang, Y. Sun, D. Men, X. Li, L. Wen, X. Lyu and Y. Li, Hierarchical hetero-Ni_3Se_4@NiFe LDH micro/nanosheets as efficient bifunctional electrocatalysts with superior stability for overall water splitting, *Nanoscale Horiz.*, 2019, **4**, 1132–1138.

15 W. Bao, L. Xiao, J. Zhang, Z. Deng, C. Yang, T. Ai and X. Wei, Interface engineering of NiV-LDH@FeOOH heterostructures as high-performance electrocatalysts for oxygen evolution reaction in alkaline conditions, *Chem. Commun.*, 2020, **56**, 9360–9363.

16 A. Meena, P. Thangavel, D. S. Jeong, A. N. Singh, A. Jana, H. Im, D. A. Nguyen, K. S. Kim, Crystalline-amorphous interface of mesoporous Ni_2P @ $FePO_xH_y$ for oxygen evolution at high current density in alkaline-anion-exchange-membrane water-electrolyzer, *Appl. Catal. B- Environ.*, 2022, **306**, 121127.

17 X. Li, M. Hou, X. Qu, Y. Zhang and M. Li, Electric-Field Assisted Hydrolysis-Oxidation of MOFs: Hierarchical Ternary (Oxy)hydroxide Micro-Flowers for Efficient Electrocatalytic Oxygen Evolution, *Small*, 2022, **18**, 2104863.
18 Y. Peng, C. Huang, J. Huang, M. Feng, X. Qiu, X. Yue and S. Huang, Filling Octahedral Interstices by Building Geometrical Defects to Construct Active Sites for Boosting the Oxygen Evolution Reaction on $NiFe_2O_4$, *Adv. Funct. Mater.*, 2022, **32**, 2201011.